PHILOSOPHICAL TRANSACTIONS A

royalsocietypublishing.org/journal/rsta

Review

Cite this article: Alexandrov DV, Galenko PK. 2020 The shape of dendritic tips. *Phil. Trans. R. Soc. A* **378**: 20190243.
http://dx.doi.org/10.1098/rsta.2019.0243

Accepted: 4 January 2020

One contribution of 18 to a theme issue 'Patterns in soft and biological matters'.

Subject Areas:
solid state physics, materials science, mathematical physics

Keywords:
dendrites, boundary integral method, heat and mass transfer, phase transformations, dendritic tips

Author for correspondence:
Peter K. Galenko
e-mail: peter.galenko@uni-jena.de

The shape of dendritic tips

Dmitri V. Alexandrov[1] and Peter K. Galenko[1,2]

[1]Department of Theoretical and Mathematical Physics, Laboratory of Multi-Scale Mathematical Modeling, Ural Federal University, Ekaterinburg 620000, Russian Federation
[2]Physikalisch-Astronomische Fakultät, Friedrich-Schiller-Universität Jena, 07743 Jena, Germany

DVA, 0000-0002-6628-745X; PKG, 0000-0003-2941-7742

The present article is focused on the shapes of dendritic tips occurring in undercooled binary systems in the absence of convection. A circular/globular shape appears in limiting cases of small and large Péclet numbers. A parabolic/paraboloidal shape describes the tip regions of dendrites whereas a fractional power law defines a shape behind their tips in the case of low/moderate Péclet number. The parabolic/paraboloidal and fractional power law shapes are sewed together in the present work to describe the dendritic shape in a broader region adjacent to the dendritic tip. Such a generalized law is in good agreement with the parabolic/paraboloidal and fractional power laws of dendritic shapes. A special case of the angled dendrite is considered and analysed in addition. The obtained results are compared with previous experimental data and the results of numerical simulations on dendritic growth.

This article is part of the theme issue 'Patterns in soft and biological matters'.

1. Introduction

A tree-like structure containing the main trunk and lateral branches that evolves in undercooled melts and supersaturated solutions is called a dendrite. The dendritic configuration of the solid material represents one of the main formations appearing during the phase transformation process from a metastable liquid state. A valuable investigation of dendritic patterns growing from supersaturated or undercooled liquids was overviewed in the works [1,2].

One of the main parameters that determine the properties of solid materials obtained by means of such phase transformations are the dendrite tip diameter, its growth velocity and the shape of the tip region. The

THE ROYAL SOCIETY PUBLISHING

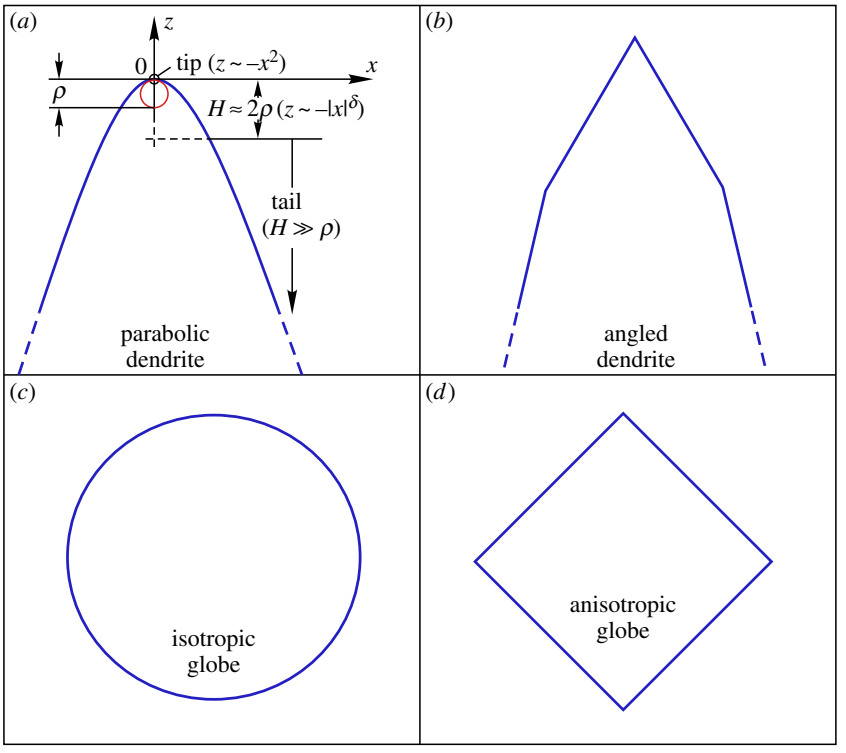

Figure 1. Various shapes of dendritic tips. Here, ρ is the dendrite tip diameter, x and z are the coordinate axes, δ is a constant power equal to 5/3 (for the two-dimensional growth of parabola) and 3/2 (for the three-dimensional growth of paraboloid) as defined in the text, and H is a characteristic distance determining the changes in the shape scaling. (Online version in colour.)

first two of them can be found using the solvability theory (see, among others, [3–10]) while the last one to date represents a difficult task for research studies.

The first attempt to find a shape of the steady-state dendrite growing in the undercooled melt was made by Ivantsov [11,12] (see also [13]). He found the shape in the form of a parabolic crystal in the two-dimensional case and of a symmetric paraboloidal crystal in the three-dimensional case. Then his theory was extended to the steady-state shape of dendritic crystal in the form of elliptical paraboloid [14–16]. An important point is that all of these solutions describe only the tip region of dendrites, which is of the order of their tip diameters. At larger distances from the dendritic vertex, the shape of the tip region changes drastically. Namely, as is shown in computations and analytical works [17–20], the tip shape is described by scaling having exponents 5/3 and 3/2, or lying closely to them. A transition region between the parabolic/paraboloidal tip and the power-dependent adjacent surface of a steady-state dendrite has never been described. This subject represents one of the main purposes of the present article. In addition, a theoretical description of circular/globular shapes and angled dendritic tips is developed below. Also, we arrange the possible tips of dendritic shapes in relation to the growth Péclet number. The developed theory is supported by mathematical derivations given in the appendixes.

A main goal of this article is to write a short overview for finally obtaining a unified analytical description of the dendritic tip that sews together the known solutions at the tip and close to it. In considering the dendritic tips, we especially analyse the case of angled dendrites appearing from the boundary integral method. This method allows us to obtain solutions for the free-boundary problems [21–26]. These shapes are discussed in the present work for weakly anisotropic dendrites in a wide range of undercooling. They are summarized in figure 1, where parabolic (a), angled (b), spherically globular (c) and angled globular (d) crystals are presented.

2. Tip shapes obtained from the boundary integral theory

The evolution of a solid–liquid interface in a binary undercooled melt can be described by a single integro-differential equation following from the boundary integral method [27,28]

$$-\frac{Q}{m_0 c_p}\left[\Delta-\frac{d_c}{\rho}K-\beta V\left(1+\frac{\partial\zeta\,(\mathbf{x},t)}{\partial t}\right)-I_\zeta^T\right]-C_{l\infty}=I_\zeta^C, \tag{2.1}$$

where $\zeta(\mathbf{x},t)$ represents the interface function, and $\mathbf{x}$ and t are the spatial and time variables. Here, Q and c_p stand for the latent heat of phase transition and the specific heat, respectively, m_0 is the liquidus slope, $\Delta=(T_f-T_{l\infty})c_p/Q$ is the melt undercooling, T_f is the phase transition temperature for a planar solid–liquid interface, $T_{l\infty}$ and $C_{l\infty}$ are the temperature and solute concentration far from the phase transition interface, ρ is a characteristic length scale of the moving interface (e.g. the diameter of a dendritic tip), β is the anisotropic kinetic coefficient, V is the steady-state growth rate and K is the interface curvature, which is defined by

$$K(\zeta)=-\frac{\partial^2\zeta/\partial x^2}{\left[1+(\partial\zeta/\partial x)^2\right]^{3/2}}\quad\text{and}\quad K(\zeta)=-\nabla\cdot\left[\frac{\nabla\zeta}{\sqrt{1+(\nabla\zeta)^2}}\right] \tag{2.2}$$

in the two- and three-dimensional geometry, respectively. The temperature and solute concentration boundary integrals I_ζ^T and I_ζ^C take the form [27,28]

$$\left.\begin{aligned}
I_\zeta^T&=P_T^{n/2}\int_0^\infty\frac{d\tau}{(2\pi\tau)^{n/2}}\int\cdots\int_\Omega\left[1+\frac{\partial\zeta\,(\mathbf{x}_1,t-\tau)}{\partial t}\right]\exp\left[-\frac{P_T}{2\tau}\Sigma\,(\mathbf{x},\mathbf{x}_1,t,\tau)\right]d^{n-1}x_1,\\
I_\zeta^C&=(1-k_0)\,P_C^{n/2}\int_0^\infty\frac{d\tau}{(2\pi\tau)^{n/2}}\int\cdots\int_\Omega C_i\,(\mathbf{x}_1,t-\tau)\\
&\quad\times\left[1+\frac{\partial\zeta\,(\mathbf{x}_1,t-\tau)}{\partial t}\right]\exp\left[-\frac{P_C}{2\tau}\Sigma\,(\mathbf{x},\mathbf{x}_1,t,\tau)\right]d^{n-1}x_1\\
\text{and}\quad&\Sigma\,(\mathbf{x},\mathbf{x}_1,t,\tau)=|\mathbf{x}-\mathbf{x}_1|^2+[\zeta\,(\mathbf{x},t)-\zeta\,(\mathbf{x}_1,t-\tau)+\tau]^2,\ C_i\,(\mathbf{x},t)=I_\zeta^C+C_{l\infty}.
\end{aligned}\right\} \tag{2.3}$$

Here, k_0 is the partition coefficient, $P_T=\rho V/(2D_T)$ and $P_C=\rho V/(2D_C)$ are the thermal and solutal Péclet numbers, D_T and D_C are the thermal and solutal diffusivities, $n=2$ and $n=3$ in two- and three-dimensional cases, respectively. Note that the vector $\mathbf{x}$ has two spatial coordinates x and y in three dimensions, $\mathbf{x}=(x,y)$, and the integration area Ω extends from minus to plus infinity in all its directions.

Expressions (2.1)–(2.3) are written in the dimensionless form which is used in the whole text of the present work.

(a) The circular and globular tip shapes at small and large Péclet numbers

To determine the circular and globular tip shapes (figure 1*c*), we use the fact that the thermal (I_ζ^T) and solutal (I_ζ^C) boundary integrals asymptotically vanish in two limiting cases of small ($P_T\to 0$ and $P_C\to 0$) and large ($P_T\to\infty$ and $P_C\to\infty$) Péclet numbers. Indeed, we have from the boundary integral equation (2.1) in the steady-state crystallization regime (when the interface function ζ does not depend on time)

$$-\frac{Q}{m_0 c_p}\left[\Delta-\frac{d_c}{\rho}K-\beta V\right]=C_{l\infty}. \tag{2.4}$$

Now, expressions (2.2) and (2.4) determine the shape of a solid–liquid interface. Note that they can be easily integrated in both two- and three-dimensional geometries under consideration. For the sake of simplicity, we will not dwell on this point here and refer the reader to our previous review article (see §7 in [28]). The main result following from these limiting cases is that the dendritic

shape represents the circular (2D case) and globular (3D case) shapes in small and large Péclet number limits. The branches of these shapes are determined as [28]

$$\left.\begin{aligned}\zeta\,(x) &= \zeta_0 + \frac{1}{B}\sqrt{1-(C_0-Bx)^2}\\ \text{and}\qquad \zeta\,(x,y) &= \zeta_0 + \frac{2}{B}\sqrt{1-\left(C_x-\frac{Bx}{2}\right)^2-\left(C_y-\frac{By}{2}\right)^2}\end{aligned}\right\} \tag{2.5}$$

in two- and three-dimensional processes, respectively. Here ζ_0, C_0, C_x and C_y are constants, and

$$B=\frac{\rho}{d_c}\left(\Delta-\beta V+\frac{m_0 C_{l\infty}c_p}{Q}\right).$$

(b) The parabolic and paraboloidal tip shapes (Ivantsov solutions)

To determine the parabolic and paraboloidal shapes, (figure 1*a*), the boundary integrals (2.3) can be explicitly evaluated if the dendritic tip represents a parabolic (in 2D case) or paraboloidal (in 3D case) shape and dendritic growth occurs in the steady-state manner when $\partial\zeta/\partial t$ in (2.1) and (2.3) vanishes. To do this, we must change the variable of integration as

$$\left.\begin{aligned}\omega &= \frac{(x-x_1)^2}{2\tau}\ \text{in 2D}\\ \text{and}\qquad \omega &= \frac{(x-x_1)^2}{2\tau},\ z_1=\frac{y-y_1}{x-x_1}\ \text{in 3D}\end{aligned}\right\} \tag{2.6}$$

and carry out mathematical manipulations lying beyond the scope of this section (see, for details, [29,30] and appendix A). Omitting the mathematical details, we obtain

$$\left.\begin{aligned}I_\zeta^T &= \sqrt{-\frac{\pi P_T}{2a}}\exp\left(-\frac{P_T}{2a}\right)\operatorname{erfc}\left(\sqrt{-\frac{P_T}{2a}}\right)\\ \text{and}\qquad I_\zeta^C &= \frac{(1-k_0)\,C_{l\infty}\tilde{f}\,(P_C)}{1-(1-k_0)\,\tilde{f}\,(P_C)},\quad \tilde{f}\,(P_C)=\sqrt{-\frac{\pi P_C}{2a}}\exp\left(-\frac{P_C}{2a}\right)\operatorname{erfc}\left(\sqrt{-\frac{P_C}{2a}}\right)\end{aligned}\right\} \tag{2.7}$$

for the two-dimensional dendritic growth with the interface function $\zeta(x)=ax^2+bx+c$ $(a<0)$, and

$$\left.\begin{aligned}I_\zeta^T &= -\frac{P_T}{2a}\exp\left(-\frac{P_T}{2a}\right)\int_1^\infty \exp\left(\frac{P_T\eta}{2a}\right)\frac{d\eta}{\eta}\\ \text{and}\qquad I_\zeta^C &= \frac{(1-k_0)\,C_{l\infty}\tilde{g}\,(P_C)}{1-(1-k_0)\,\tilde{g}\,(P_C)},\quad \tilde{g}\,(P_C)=-\frac{P_C}{2a}\exp\left(-\frac{P_C}{2a}\right)\int_1^\infty \exp\left(\frac{P_C\eta}{2a}\right)\frac{d\eta}{\eta}\end{aligned}\right\} \tag{2.8}$$

for the three-dimensional dendritic growth with the interface function $\zeta(x,y)=a(x^2+y^2)+b(x+y)+c$ $(a<0)$. Here a, b and c represent the constants that determine the parabolic (paraboloidal) shapes.

Now neglecting the curvature term in equation (2.1) and using the boundary integrals (2.7) or (2.8), we come to the following expression that defines the melt undercooling ahead of the growing dendritic tip with allowance for the steady-state regime

$$-\frac{Q}{m_0 c_p}\left[\Delta-\beta V-I_\zeta^T\right]-C_{l\infty}=I_\zeta^C. \tag{2.9}$$

Expression (2.9) describes the two- and three-dimensional solidification regimes in which I_ζ^T and I_ζ^C are given by formulae (2.7) or (2.8).

Thus, the parabolic (paraboloidal) shapes found for the first time by Ivantsov represent approximate solutions of the boundary integral equation (2.1). These solutions well work in those parametric regions where the interface curvature (2.2) is small enough so that the term d_cK/ρ does not give a sufficient contribution in the square brackets of expression (2.1).

(c) Angled tips of dendrites

The boundary integrals (2.3) can also be evaluated if we are dealing with the case of so-called angled dendrites (figure 1*b*). This case describes a spike shape of two- and three-dimensional dendritic tips frequently met in various applications. As before, for the sake of clearer presentation, we refer to the mathematical treatments given in appendix B. The final result at $x \to 0$ and $y \to 0$ (near the dendritic tip) can be obtained in the form of

$$I_\zeta^T = \frac{2}{\pi}\arctan\left(-\frac{1}{a}\right), \quad I_\zeta^C = \frac{(1-k_0)\,C_{l\infty}I_\zeta^T}{1-(1-k_0)\,I_\zeta^T}, \quad a<0 \tag{2.10}$$

for a two-dimensional angled dendrite with the interface function $\zeta(x) = a|x| + b$ $(a < 0)$, and

$$\left.\begin{aligned} I_\zeta^T &= \frac{1}{\pi\sqrt{1+a^2}}\int_0^\infty\left\{\int_0^\infty \exp\left[-(1+\kappa')\omega'\right]\operatorname{erfc}\left[-\sqrt{\omega'}\chi'\right]\mathrm{d}x_1'\right\}\frac{d\omega'}{\omega'} \\ \text{and}\quad I_\zeta^C &= \frac{(1-k_0)\,C_{l\infty}I_\zeta^T}{1-(1-k_0)\,I_\zeta^T},\ \chi'\left(x_1',\omega'\right) = \frac{a\left(a-x_1'/(2\omega')\right)}{\sqrt{1+a^2}},\ \kappa'\left(x_1',\omega'\right) = \frac{\chi'^2\left(x_1',\omega'\right)}{a^2},\ a<0 \end{aligned}\right\} \tag{2.11}$$

for a three-dimensional angled dendrite with the interface function $\zeta(x,y) = a(|x| + |y|) + b$ $(a < 0)$. Here, the constants a and b describe a shape of angled dendrites. It is important to emphasize that the thermal and concentration integrals (2.10) and (2.11) are independent of the Péclet numbers P_T and P_C in the case of two- and three-dimensional angled dendrites.

Note that, due to the sharp tip of the angled dendrite, its interface curvature is absent and the boundary integral (2.1) determines the melt undercooling ahead of the dendritic tip (where I_ζ^T and I_ζ^C are defined by formulae (2.10) and (2.11)). The obtained angled tips of dendrites differ considerably from their faceted tips. The angled dendrite appears as a solution of boundary integral that exists in a whole range of undercooling and for any value of crystalline anisotropy. Faceted dendrites are formed due to increased anisotropy of interface energy which predominantly acts in the smallest and intermediate range of undercooling.

Thus, the thermal and solutal boundary integrals, I_ζ^T and I_ζ^C, can be analytically evaluated to obtain circular/globular, parabolic/paraboloidal and angled dendritic shapes. The next paragraph is concerned with the shapes of tip regions of growing dendrites obtained by means of computer simulations.

3. Dendritic shapes obtained from computations

Real dendritic crystals represent complex branching patterns whose shape differs from ideal shapes described in the previous section. If we are dealing with a wide range of possible Péclet numbers the shape of tip regions differs from Ivantsov parabolas (paraboloids) in close proximity to the dendrite tips. To find such shapes, we need to use more complex mathematical tools than purely analytical techniques, which are based on computer simulations of spatial and time scalings of dendritic tips in the same way as was done in pioneering articles by Almgren, Dai & Hakim [17] (two-dimensional dendrites) and Plapp & Karma [18] (three-dimensional dendrites). Below we briefly discuss their results in terms of dendritic shapes.

(a) Two-dimensional dendrites

Using the boundary integral theory and direct numerical simulations, Almgren *et al*. [17] showed that the two-dimensional dendritic arms develop in such a manner that their lengths and widths grow in time as $t_d^{3/5}$ and $t_d^{2/5}$, respectively (here, t_d designates the dimensionless time variable).

Then, using this scaling behaviour, Brener showed that the shape of dendritic tips takes the form [19,20]

$$z_B(x) = \alpha |x|^{5/3}, \tag{3.1}$$

where α is a constant, and z_B and x represent the spatial coordinates along to and perpendicular to the direction of dendritic tip's growth, respectively.

It is significant that experiments carried out by Bisang & Bilgram [31] confirm the shape given by expression (3.1). Namely, they showed that the Ivantsov solutions (parabolas or paraboloids) work only very near to the dendritic tip regions. As the distance from the tip becomes of the order of dendritic diameter ρ, a dendritic shape becomes in agreement with the shape (3.1).

(b) Three-dimensional dendrites

A novel computational method based on a multiscale random-walk algorithm was developed by Plapp & Karma [18] to simulate three-dimensional dendritic growth. They showed that the scaling law (3.1) must be changed in the case of three-dimensional axisymmetric dendritic growth by the following formula:

$$z_{PK}(x) = \alpha |x|^{3/2}, \tag{3.2}$$

where all designations correspond to expression (3.1) and x represents the spatial coordinate of a symmetrically growing dendrite.

Physically, the scaling laws (3.1) and (3.2) are different due to the fact that the tip velocity is much larger in the three-dimensional case than in the two-dimensional case. The latter is caused by the fact that the heat- and mass transfer equations, as well as boundary conditions in 3D and 2D, have a different form, which is dictated by various Lamé coefficients [32,33].

To conclude this section, we stress the fact that the Ivantsov solutions work only at the dendritic tip and in a very small vicinity around the tip, but the scaling laws (3.1) and (3.2) determine the shape of the neighbouring area to the dendrite tip.

4. Sewing together various tip shapes

In this section, we present the analytical expressions for dendritic shapes obtained by the method of sewing together two different solutions: the Ivantsov parabolic shape (paraboloidal shape in three dimensions) valid at the dendritic tip and the power law (3.1) (or the power law (3.2) in three-dimensional case) valid at a distance of the order of several tip diameters from the dendritic vertex.

(a) Two-dimensional dendritic shapes

Let us now sew together the two-dimensional Ivantsov solution $z_{Iv}(x) = -x^2$, which formally takes place at small arguments $x \to 0$, and the power shape (3.1), which is valid at increased values of the argument x (or formally at $x \gg 1$). Keeping this in mind, assuming for simplicity that $\alpha = -1$ (this can always be done by rescaling [31]), and choosing the fractional function for sewing, we finally obtain

$$z_{AG}(x) = -\frac{b_S(x)x^2 + b_L(x)|x|^{5/3}}{b_S(x)|x|^{1/3} + b_L(x)|x|^{-1/3}} \quad \text{two-dimensional dendrite,} \tag{4.1}$$

where $b_S(x)$ and $b_L(x)$ are the arbitrary functions satisfying the formal sewing conditions

$$\left.\begin{aligned} &b_S(x) \to 0,\ b_L(x) \to 1 \text{ at } x \to 0 \\ \text{and} \quad &b_S(x) \to 1,\ b_L(x) \to 0,\ \text{at } x \gg 1. \end{aligned}\right\} \tag{4.2}$$

It is significant to note the limiting cases of small and large values of x following from the generalized expression (4.1). Namely, if x is small enough, we come to the Ivantsov solution

$$z_{AG}(x) \approx -\frac{b_L(x)|x|^{5/3}}{b_L(x)|x|^{-1/3}} = -x^2, \ x \to 0. \tag{4.3}$$

On the other hand, if x is large enough, we arrive at Brener's solution

$$z_{AG}(x) \approx -\frac{b_S(x)x^2}{b_S(x)|x|^{1/3}} = -|x|^{5/3}, \ x \gg 1. \tag{4.4}$$

Let us now write out possible functions $b_S(x)$ and $b_L(x)$, which satisfy the sewing conditions (4.2) and, what is more important, lead to a good approximation of dendritic shape for a broad range of x. Indeed, we can simply choose them as

$$b_S(x) = \exp\left(-\frac{1}{x^{2k}}\right) \quad \text{and} \quad b_L(x) = \exp\left(-x^{2k}\right), \tag{4.5}$$

where k is a positive integer which determines the smoothness of the transition from Ivantsov's solution to Brener's solution.

Figure 2 compares the solution (4.1) for the dendritic shape with two previously known asymptotic solutions presented by Ivantsov $z_{Iv}(x)$ and by Brener $z_B(x)$. As is easily seen, $z_{AG}(x)$ (green dots) merges with the Ivantsov function $z_{Iv}(x)$ (blue dashed line) at small x in the dendritic tip region (compare the dotted and dashed lines shown in figure 2*a*). When x becomes large enough, $z_{AG}(x)$ (green dots) actually coincides with the Brener function $z_B(x)$ (red solid line), which describes the shape at some distance from the dendritic vertex (compare the dotted and solid lines illustrated in figure 2*c*). The intermediate region, where the shape changes from the Ivantsov solution to the Brener one, is demonstrated in figure 2*b*. Here, we can easily see that the new function $z_{AG}(x)$ (green dots) smoothly changes the shape function from $z_{Iv}(x)$ (at the tip region) to $z_B(x)$ (at some distance from it). Thus, the function (4.1) describes the shapes of two-dimensional dendrites in a broad diapason of spatial coordinates ranging from a tip region to a peripheral one. The latter is shown by the *tail* region in figure 1*a*.

(b) Three-dimensional dendritic shapes

Let us now consider some cross-section of a symmetrically growing three-dimensional dendrite so that the problem reduces to the two-dimensional case, where the tip region is described by the Ivantsov function $z_{Iv}(x) = -x^2$, and the region behind its tip is defined by the Plapp & Karma shape (3.2) with $\alpha = -1$. The rotation of these functions around the growth axis of the dendrite, which passes through its vertex, determines the axisymmetric surface of rotation. This case can be studied by analogy with the two-dimensional dendritic growth. Indeed, sewing together functions $z_{Iv}(x)$ and $z_{PK}(x)$, we arrive at

$$z_{AG}(x) = -\frac{b_S(x)x^2 + b_L(x)|x|^{3/2}}{b_S(x)|x|^{1/2} + b_L(x)|x|^{-1/2}} \quad \text{three-dimensional dendrite,} \tag{4.6}$$

where, as before, $b_S(x)$ and $b_L(x)$ satisfy the sewing conditions (4.2). Note that this function respectively tends to the Ivantsov and Plapp-Karma solutions in the limiting cases of small and large arguments, that is

$$\left.\begin{aligned} z_{AG}(x) &\approx -\frac{b_L(x)|x|^{3/2}}{b_L(x)|x|^{-1/2}} = -x^2, \quad x \to 0 \\ \text{and} \qquad z_{AG}(x) &\approx -\frac{b_S(x)x^2}{b_S(x)|x|^{1/2}} = -|x|^{3/2}, \quad x \gg 1. \end{aligned}\right\} \tag{4.7}$$

The functions $b_S(x)$ and $b_L(x)$ can be chosen accordingly to expressions (4.5).

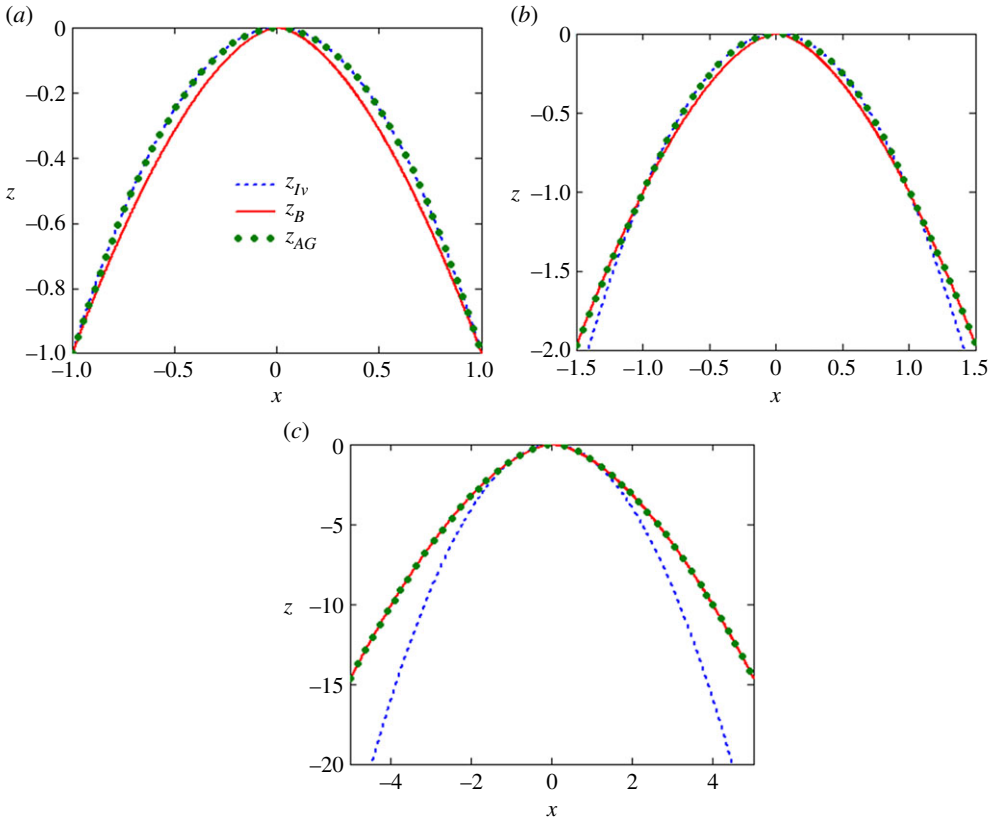

Figure 2. Dendritic shapes given by the Ivantsov solution $z_{Iv}(x) = -x^2$ (blue dashed line), the Brener solution $z_B(x)$ (red solid line, expression (3.1)), and the generalized solution $z_{AG}(x)$ (green dotted line, expression (4.1)). The Ivantsov and Brener functions, respectively, describe the shape of dendrite very near to its vertex (*a*) and at some distance from it (*c*). The intermediate region (*b*) as well as two regions shown in (*a*) and (*c*) are well described by the $z_{AG}(x)$-solution plotted at $k = 3$. (Online version in colour.)

The behaviour of three-dimensional solutions is shown in figure 3. Here, figure 3*a* demonstrates a dendritic cross-sectional area (intermediate region only) in accordance with the Ivantsov function, $z_{Iv}(x) = -x^2$, the Plapp and Karma function (3.2), and the generalized solution (4.6). As is seen, the generalized solution agrees well with two asymptotic regimes. The behaviour of solutions in the rest regions (near a dendritic vertex and far from it) is completely analogous to the two-dimensional case (figure 2*a*,*c*). Figure 3*b* illustrates the shape of a three-dimensional dendrite obtained by means of rotation of the generalized solution (4.6) around the growth axis *z*. As in the two-dimensional case, the solution (4.6) describes well all previously known shapes of three-dimensional dendritic growth derived by Ivantsov, Plapp and Karma.

(c) Two- and three-dimensional dendritic shapes: a generalized law

The two- and three-dimensional dendritic shapes (4.1) and (4.6) can be generalized and written out as a single law determining the shape of dendrites near their tip regions in the form of

$$z_{AG}(x) = -\frac{b_S(x)x^2 + b_L(x)|x|^{(9-2n)/(5-n)}}{b_S(x)|x|^{1/(5-n)} + b_L(x)|x|^{-\frac{1}{5-n}}} \quad \text{two- and three-dimensional dendrites,} \tag{4.8}$$

where $n = 2$ and $n = 3$ for two- and three-dimensional dendritic shapes. Note that $b_S(x)$ and $b_L(x)$, as before, satisfy the sewing conditions (4.2) and can be chosen accordingly to expressions (4.5).

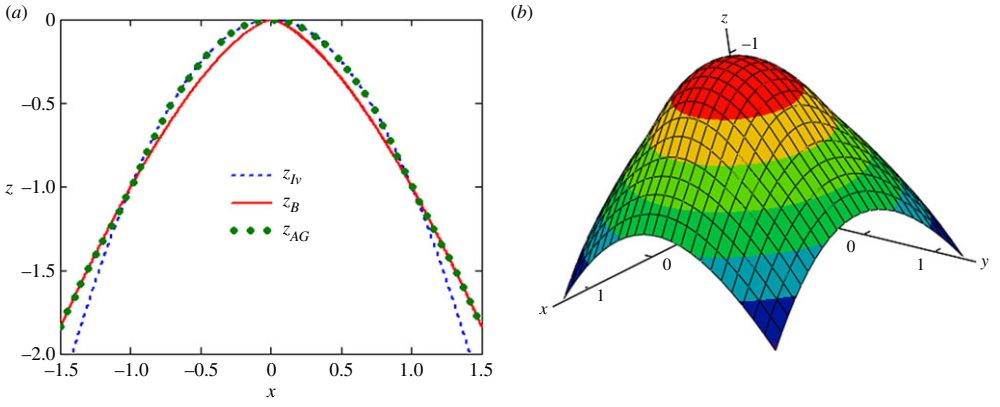

Figure 3. (*a*) Dendritic shapes given by the Ivantsov solution $z_{Iv}(x) = -x^2$ (blue dashed line), the Plapp & Karma solution $z_{PK}(x)$ (red solid line, expression (3.2)) and the generalized solution $z_{AG}(x)$ (green dotted line, expression (4.6)) in the intermediate region. The Ivantsov and Plapp-Karma functions, respectively, describe the shape of dendrite very near to its vertex and at some distance from it. (*b*) A three-dimensional shape plotted according to the generalized solution $z_{AG}(x)$ at $k = 3$, (expression (4.6)). (Online version in colour.)

5. Discussion and conclusion

The aforementioned shapes of dendritic tip regions are summarized in table 1. Let us briefly discuss below the main points following from our analysis.

First of all, the boundary integral (2.1) has an identical asymptotic solution in two cases of small and great Péclet numbers P_T and P_C. Indeed, if $P_T \to 0$ and $P_C \to 0$ (or $P_T \to \infty$ and $P_C \to \infty$), the thermal and concentration integrals I_ζ^T and I_ζ^C vanish and equation (2.1) can be explicitly integrated. Namely, its integration leads to a circular/globular shape given by expression (2.5). This law describes the crystals that are capable of nucleating and growing in the bulk of undercooled melt or supersaturated solution.

In the second instance, a parabolic/paraboloidal shape takes place only in the dendritic tip region at a low/moderate Pécle number if the surface tension is negligible. In addition, a characteristic distance measured from the dendrite vertex where the shape can be considered as parabolic/paraboloidal is of the order of the radius of curvature. If this is really the case, the boundary integral (2.1) should be integrated in the absence of interface curvature K that leads to the undercooling balance in the form of expression (2.9).

In the third instance, the tip surface changes its shape with increasing distance from the dendritic vertex. Namely, when we are at the greater distance (in order of magnitude) from the dendrite tip radius, the shape is described by a fractional power law. Such a power-dependent law works at the distance that is less (in order of magnitude) than several dendrite tip radii. In this region, the approximate power-law (3.1), deduced by Brener on the basis of two-dimensional computations [17], takes place. His law $z_B(x) = \alpha|x|^{5/3}$ was tested against three-dimensional experimental data on xenon dendrites by Bisang & Bilgram [31] and on succinonitrile dendrites grown in microgravity conditions by Li & Beckermann [47]. Their works show that the power law (3.1) works well behind the tip region. What is more, three-dimensional computations of dendritic growth carried out by Plapp & Karma [18] lead to another power-dependent law $z_{PK} = \alpha|x|^{3/2}$. As we know, their law has never been tested against experiments or numerical simulations. However, both powers 5/3 and 3/2 lie close to each other and the difference between them can be of the order of experimental or computational error. In this respect experiments with three-dimensional chemical dendrites grown from supersaturated aqueous solutions NH_4Cl show that the shape of the region around the dendrite tip also has the power of 5/3 [52]. More accurate studies of the feasibility of the aforementioned power-laws in a broad range of growth regimes represent a challenging problem for future investigations.

Table 1. Summary of known shapes near dendritic tips (here α is a shape constant). Here, we treat $P_T \lesssim 10^{-3}$ as small, $P_T \sim 10^{-3} - 10^{-2}$ as moderate, and $P_T \gtrsim 10^{-2}$ as high Péclet numbers.

2D/3D shapes	limitation	theory	experiments or computations
circular/globular	vanishing Péclet	§2a	[34–38]
anisotropic globular	vanishing Péclet	§2a	[34,37–41]
parabolic/paraboloidal, $z = \alpha x^2, z = \alpha(x^2 + y^2)$	low/moderate Péclet, zero surface tension	§2b, [15,27,45,46]	[35,42–44]
power, $z = \alpha \lvert x\rvert^{5/3}, z = \alpha \lvert x\rvert^{3/2}$	low/moderate Péclet	[17–19]	[31,47,48]
angled, $z = \alpha \lvert x\rvert, z = \alpha(\lvert x\rvert + \lvert y\rvert)$	—	§2c	[49,50]
anisotropic globular	highest Péclet	[28,51]	[36–38,41]
circular/globular	highest Péclet	[28,51]	[37,38,41]
generalized power, (4.1), (4.6), (4.8)	low/moderate Péclet	§4	sewed limits are tested in [31,35,42–44,47]

In the fourth instance, the power laws suggested by Brener (computed/derived in 2D and verified in 3D) and by Plapp & Karma (computed in 3D) that are valid at some distance from the dendritic vertex have been sewed together with the parabolic/paraboloidal shapes valid in the vertex region only (section 4). We show that our solutions (expressions (4.1) and (4.6)) coincide well with the parabolic/paraboloidal shapes in the tip region and with the aforementioned power laws behind it. In addition, a generalized power law (4.8) joining together the two- and three-dimensional cases is found. Checking the feasibility of generalized power shapes (4.1), (4.6) and (4.8) in future experiments and numerical simulations is an additional challenging task.

In the last instance, we demonstrate that the boundary integral theory contains the angled-type dendrites as possible solutions of two- and three-dimensional problems (§2c). Taking into account previous theory and simulations [49,50], we are able to conclude that such dendrites grow at certain undercoolings that determine their tip angles. It is remarkable that the angled dendrites exist as the solutions of the boundary integral method in a whole spectrum of undercoolings (small, moderate and high). In this respect, one can mention the experimental work of Maurer *et al.* [53], where the so-called facetted dendrites of NH_4Br crystals were obtained for vanishing growth velocities, i.e. smallest supersaturation. Usually, facetted dendrites appear due to the high anisotropy of surface energy or atomic kinetics. However, dendrites that are grown from the aqueous solution of NH_4Br should exhibit small anisotropy of interface properties (surface energy and growth kinetics). Therefore, one can also attribute these experimental data from Maurer *et al.* to the case of growth of angled dendrites at vanishing supersaturation. More detailed studies of such angled structures are also required in the future to establish their properties and growth laws.

Concluding this section, let us especially emphasize that the present article does not represent a comprehensive review of possible tip shapes appearing in dendritic growth. So, for example, such phenomena as convection, local non-equilibrium effects, gravitational and electromagnetic fields, and chemical interaction between atoms that completely change the growth conditions and dendritic shapes can be included in the further analysis. Questions related to the shape of dendrites away from their tip regions, splitting of their tips, morphological instability and sidebranches in dendritic growth lie outside the scope of the present article as well.

Data accessibility. This article does not contain any additional data.
Authors' contributions. All authors contributed equally to this study.

Competing interests. We declare we have no competing interests.
Funding. Authors thank Efim Brener and Mathis Plapp for the fruitful discussions. This work was supported by the Russian Science Foundation (grant no. 16-11-10095).

Appendix A. Boundary integrals for parabolic and paraboloidal dendrites

The thermal and concentration integrals I_ζ^T and I_ζ^C from (2.3) in the case of steady-state dendritic growth can be written as ($C_i = C_{l\infty} + I_\zeta^C$)

$$\left.\begin{aligned} I_\zeta^T &= P_T \int_0^\infty \frac{d\tau}{2\pi\tau} \int_{-\infty}^{\infty} \exp\left[-\frac{P_T}{2\tau}\Sigma(x,x_1,\tau)\right] \mathrm{d}x_1, \\ I_\zeta^C &= (1-k_0)P_C \int_0^\infty \frac{d\tau}{2\pi\tau} \int_{-\infty}^{\infty} C_i(x_1) \exp\left[-\frac{P_C}{2\tau}\Sigma(x,x_1,\tau)\right] \mathrm{d}x_1 \\ \text{and} \quad \Sigma(x,x_1,\tau) &= (x-x_1)^2 + [\zeta(x)-\zeta(x_1)+\tau]^2, \end{aligned}\right\} \tag{A 1}$$

in the case of two-dimensional growth, and

$$\left.\begin{aligned} I_\zeta^T &= P_T^{3/2} \int_0^\infty \frac{d\tau}{(2\pi\tau)^{3/2}} \int_{-\infty}^{\infty}\int_{-\infty}^{\infty} \exp\left[-\frac{P_T}{2\tau}\Sigma(\mathbf{x},\mathbf{x}_1,\tau)\right] d^2x_1, \\ I_\zeta^C &= (1-k_0)P_C^{3/2} \int_0^\infty \frac{d\tau}{(2\pi\tau)^{3/2}} \int_{-\infty}^{\infty}\int_{-\infty}^{\infty} C_i(\mathbf{x}_1) \exp\left[-\frac{P_C}{2\tau}\Sigma(\mathbf{x},\mathbf{x}_1,\tau)\right] d^2x_1 \\ \text{and} \quad \Sigma(\mathbf{x},\mathbf{x}_1,\tau) &= |\mathbf{x}-\mathbf{x}_1|^2 + [\zeta(\mathbf{x})-\zeta(\mathbf{x}_1)+\tau]^2, \end{aligned}\right\} \tag{A 2}$$

in the case of three-dimensional growth.

(a) Two-dimensional case (parabola)

Now we seek for a solution of integrals (A 1) if the interface function is given by a parabola

$$\zeta(x) = ax^2 + bx + c, \tag{A 3}$$

where $a < 0$, b, c are the constants. Now substituting $\zeta(x)$ from (A 3) into (A 1), and replacing τ by ω

$$\omega = \frac{(x-x_1)^2}{2\tau},$$

we arrive at

$$I_\zeta^T = \frac{P_T}{2\pi} \int_0^\infty \frac{d\omega}{\omega} \int_{-\infty}^{\infty} \exp\left[-P_T\omega\left(1 + \left(a(x+x_1)+b+\frac{x-x_1}{2\omega}\right)^2\right)\right] \mathrm{d}x_1. \tag{A 4}$$

Changing again the variable of integration

$$z = -\sqrt{P_T\omega}\left(a(x+x_1)+b+\frac{x-x_1}{2\omega}\right),$$

in (A 4), we integrate I_ζ^T and come to the following expression:

$$I_\zeta^T = -\frac{\sqrt{P_T}}{2\sqrt{\pi}} \int_0^\infty \frac{\exp(-P_T\omega)\, d\omega}{\sqrt{\omega}(a\omega - 1/2)}. \tag{A 5}$$

Taking into account that [54]

$$\int_0^\infty \frac{\exp(-q\alpha)}{\sqrt{\alpha}} d\alpha = \sqrt{\frac{\pi}{q}}, \quad q > 0, \tag{A 6}$$

we can integrate expression (A 5) if $a = 0$ as

$$I_\zeta^T = 1, \quad a = 0. \tag{A 7}$$

Assuming that $a \neq 0$ and rewriting (A 5) as

$$I_\zeta^T = 1 - \sqrt{\frac{P_T}{\pi}} a \int_0^\infty \frac{\sqrt{\omega}\exp(-P_T\omega)\,d\omega}{a\omega - 1/2}, \tag{A 8}$$

we can evaluate this integral by means of the following formula [54]

$$\int_u^\infty \frac{\sqrt{\alpha - u}}{\alpha}\exp(-\mu\alpha)\,d\alpha = \sqrt{\frac{\pi}{\mu}}\exp(-\mu u) - \pi\sqrt{u}\,\mathrm{erfc}\left(\sqrt{u\mu}\right), \quad u > 0,\ \mathrm{Re}(\mu) > 0.$$

This enables us to write down (A 7) and (A 8) in the form of

$$I_\zeta^T = \begin{cases} \sqrt{-\dfrac{\pi P_T}{2a}}\exp\left(-\dfrac{P_T}{2a}\right)\mathrm{erfc}\left(\sqrt{-\dfrac{P_T}{2a}}\right), & a < 0 \\ 1, & a = 0 \end{cases} \tag{A 9}$$

Note that if $a = -1/2$, the thermal integral (A 9) becomes

$$I_\zeta^T = P_T\exp(P_T)\int_1^\infty \frac{\exp(-P_T\upsilon)\,d\upsilon}{\sqrt{\upsilon}}, \tag{A 10}$$

which is identical to expressions (30) in [27] and (5.1) in [28].

The second integral I_ζ^C in (A 1) describing the binary systems can be found in the same manner as I_ζ^T. Indeed, changing P_T by P_C and keeping in mind the constant term $(1 - k_0)C_i$, we get from formulae (A1)

$$I_\zeta^C = (1 - k_0)C_i\tilde{f}(P_C) \tag{A 11}$$

and

$$\tilde{f}(P_C) = \begin{cases} \sqrt{-\dfrac{\pi P_C}{2a}}\exp\left(-\dfrac{P_C}{2a}\right)\mathrm{erfc}\left(\sqrt{-\dfrac{P_C}{2a}}\right), & a < 0 \\ 1, & a = 0. \end{cases} \tag{A 12}$$

To find the solute concentration at the solid–liquid interface $C_i = C_{l\infty} + I_\zeta^C$, we combine this formula with (A 11) and (A 12). The result takes the form

$$C_i = \frac{C_{l\infty}}{1 - (1 - k_0)\tilde{f}(P_C)}, \tag{A 13}$$

which is identical to formulae (34) in [27] and (5.8) in [28] if $a = -1/2$.

(b) Three-dimensional case (paraboloid of revolution)

Let us assume that the interface function is given by an axisymmetric paraboloid

$$\zeta(x, y) = a(x^2 + y^2) + b(x + y) + c, \tag{A 14}$$

where $a < 0$, b and c are again constants. Changing the integration variables ω and y_1 in the thermal integral (A2) as

$$\omega = \frac{(x - x_1)^2}{2\tau} \quad \text{and} \quad y - y_1 = (x - x_1)z_1, \tag{A 15}$$

we rewrite I_ζ^T in the form of

$$I_\zeta^T = -\frac{1}{2}\left(\frac{P_T}{\pi}\right)^{3/2}\int_0^\infty \frac{d\omega}{\sqrt{\omega}}\int_{-\infty}^\infty \frac{\exp\left[-P_T\omega(1 + z_1^2)\right]dz_1}{a + az_1^2 - (2\omega)^{-1}}\int_{-\infty}^\infty \exp\left(-P_T\omega u^2\right)\mathrm{d}u, \tag{A 16}$$

where

$$u = a(x + x_1) + b(1 + z_1) + az_1\left[2y - (x - x_1)z_1\right] + \frac{x - x_1}{2\omega}.$$

Keeping in mind that [54]

$$\int_0^\infty \frac{\exp\left(-\mu^2 v^2\right) \mathrm{d}v}{v^2+\beta^2} = \frac{\pi}{2\beta}\mathrm{erfc}(\beta\mu)\exp\left(\beta^2\mu^2\right),$$

we rewrite (A16) in the following form:

$$I_\zeta^T = -\frac{P_T}{a}\exp\left(-\frac{P_T}{2a}\right)\int_{1/\sqrt{-(2a)}}^\infty \frac{\mathrm{erfc}\left[\sqrt{P_T}w\right]\mathrm{d}w}{\sqrt{w^2+(2a)^{-1}}},\ w=\sqrt{\omega-(2a)^{-1}}. \tag{A 17}$$

Let us introduce the additional parameter $\alpha=\sqrt{P_T}$ to simplify the integral (A 17) such that the auxiliary function and its derivative are

$$J(\alpha)=\int_{1/\sqrt{-(2a)}}^\infty \frac{\mathrm{erfc}\left[\alpha w\right]dw}{\sqrt{w^2+(2a)^{-1}}},\ J'(\alpha)=-\frac{\exp\left[\alpha^2\left(1+(2a)^{-1}\right)\right]}{\sqrt{\pi}}\int_1^\infty \frac{\exp\left[-\alpha^2\gamma\right]\mathrm{d}\gamma}{\sqrt{\gamma-1}},$$

where $\gamma=w^2+1+(2a)^{-1}$. The integral entering in the right-hand side of $J'(\alpha)$ takes the form [54]: $\sqrt{\pi}\exp(-\alpha^2)/\alpha$. This enables us to rewrite $J'(\alpha)$ as

$$J'(\alpha)=-\frac{1}{\alpha}\exp\left[\frac{\alpha^2}{2a}\right].$$

Integrating $J'(\alpha)$ with allowance for the boundary condition $J(\alpha)\to 0$ within the limit $\alpha\to\infty$, we arrive at

$$J(\alpha)=\int_\alpha^\infty \exp\left[\frac{\nu^2}{2a}\right]\frac{\mathrm{d}\nu}{\nu}.$$

Combining $J(\alpha)$ and (A17) and changing the variable as $\nu=\sqrt{P_T\eta}$, we come to the following expression:

$$I_\zeta^T = -\frac{P_T}{2a}\exp\left[-\frac{P_T}{2a}\right]\int_1^\infty \exp\left[\frac{P_T\eta}{2a}\right]\frac{\mathrm{d}\eta}{\eta}, \tag{A 18}$$

which is identical to formulae (31) in [27] and (5.5) in [28] if $a=-1/2$.

If $a=0$, the integral (A 18) can be found directly from (A 16) as $I_\zeta^T=1$ at $a=0$. Keeping this in mind, I_ζ^T reads as

$$I_\zeta^T=\begin{cases}-\dfrac{P_T}{2a}\exp\left[-\dfrac{P_T}{2a}\right]\displaystyle\int_1^\infty \exp\left[\frac{P_T\eta}{2a}\right]\frac{d\eta}{\eta}, & a<0\\ 1, & a=0\end{cases}. \tag{A 19}$$

To easily evaluate I_ζ^C, we should again change P_T by P_C and take into consideration the constant concentration difference $(1-k_0)C_i$. This enables us to express I_ζ^C as

$$I_\zeta^C=(1-k_0)C_i\tilde{g}(P_C) \tag{A 20}$$

and

$$\tilde{g}(P_C)=\begin{cases}-\dfrac{P_C}{2a}\exp\left[-\dfrac{P_C}{2a}\right]\displaystyle\int_1^\infty \exp\left[\frac{P_C\eta}{2a}\right]\frac{d\eta}{\eta}, & a<0\\ 1, & a=0\end{cases}. \tag{A 21}$$

The solid–liquid concentration $C_i=C_{l\infty}+I_\zeta^C$ in this case is found by means of formulae (A 20) and (A 21) in the form of

$$C_i=\frac{C_{l\infty}}{1-(1-k_0)\tilde{g}(P_C)}, \tag{A 22}$$

which is identical to formulae (34) in [27] and (5.8) in [28] for $a=-1/2$.

Appendix B. Boundary integrals for angled dendrites

(c) Two-dimensional case

Let us assume that a two-dimensional angled dendrite with the interface function $\zeta(x) = a|x| + b$ ($a < 0$ and b represent constants) evolves in a two-component liquid with a constant velocity. To evaluate the thermal integral in (2.3), we divide it into two contributions, i.e.

$$I_\zeta^T = P_T \int_0^\infty \frac{d\tau}{2\pi\tau} \left(\int_0^\infty + \int_{-\infty}^0 \right) \exp\left[-\frac{P_T}{2\tau} \Sigma(x, x_1, \tau) \right] \mathrm{d}x_1. \tag{B1}$$

The first of these integrals with respect to x_1 changing from 0 to ∞ can be calculated by means of the following interface function $\zeta(x_1) = ax_1 + b$, and

$$\Sigma(x, x_1, \tau) = (x - x_1)^2 + [a(x - x_1) + \tau]^2.$$

Replacing the variable of integration in (B1) with respect to τ as $\omega = (x - x_1)^2/(2\tau)$ and substituting u instead of x_1 as $u = -\sqrt{P_T\omega}[a + (x - x_1)/(2\omega)]$, we come to the first contribution in expression (B1)

$$\frac{\sqrt{P_T}}{2\sqrt{\pi}} \int_0^\infty \frac{\exp(-P_T\omega)}{\sqrt{\omega}} \mathrm{erfc}\left[-\sqrt{P_T\omega} \left(a + \frac{|x|}{2\omega} \right) \right] \mathrm{d}\omega. \tag{B2}$$

The second of integrals in expression (B1) with respect to x_1 changing from $-\infty$ to 0 should be calculated with

$$\zeta(x_1) = -ax_1 + b \quad \text{and} \quad u = \sqrt{P_T\omega} \left(\frac{x - x_1}{2\omega} - a \right).$$

The final result coincides with (B2). Keeping this in mind, the thermal integral (B1) takes the form

$$I_\zeta^T = \sqrt{\frac{P_T}{\pi}} \int_0^\infty \frac{\exp(-P_T\omega)}{\sqrt{\omega}} \mathrm{erfc}\left[-\sqrt{P_T\omega} \left(a + \frac{|x|}{2\omega} \right) \right] \mathrm{d}\omega. \tag{B3}$$

The integral (B3) can be simplified in the dendritic tip region $|x| \to 0$ as

$$I_\zeta^T = \sqrt{\frac{P_T}{\pi}} \int_0^\infty \frac{\exp(-P_T\omega)}{\sqrt{\omega}} \mathrm{erfc}\left(-a\sqrt{P_T\omega} \right) \mathrm{d}\omega = \frac{2}{\pi} \arctan\left(-\frac{1}{a} \right). \tag{B4}$$

Note that the thermal integral (B4) describing the case of two-dimensional angled dendrite does not depend on Péclet number $P_T = \rho V/(2D_T)$.

The concentration integral I_ζ^C from (2.3) can be evaluated in the same manner as I_ζ^T. The result is $I_\zeta^C = (1 - k_0)C_i I_\zeta^T$. Now taking into account that $C_i = I_\zeta^C + C_{l\infty}$, we get expressions (2.10).

(d) Three-dimensional case

We now evaluate the thermal integral (2.3) in the three-dimensional geometry, where the interface function for an angled dendrite is given by $\zeta(x, y) = a(|x| + |y|) + b$ ($a < 0$ and b are constants).

For the sake of convenience, we divide the integral I_ζ^T in (2.3) into four parts. The first of them is determined by the interface function $\zeta(x, y) = a(x + y) + b$ ($x > 0$, $y > 0$), and

$$\Sigma(x, y) = (x - x_1)^2 + (y - y_1)^2 + [a(x - x_1) + a(y - y_1) + \tau]^2.$$

Replacing τ by ω and y_1 by z_1 as

$$\tau = \frac{(x - x_1)^2}{2\omega}, \; y_1 = y + (x - x_1)z_1,$$

we obtain the following contribution to I_ζ^T:

$$\frac{P_T^{3/2}}{2\pi^{3/2}} \int_0^\infty \int_0^\infty \int_{-y/(x-x_1)}^\infty \exp\left\{ -P_T\omega \left[1 + z_1^2 + \left(a - az_1 + \frac{x - x_1}{2\omega} \right)^2 \right] \right\} \mathrm{d}z_1 \mathrm{d}x_1 \frac{\mathrm{d}\omega}{\sqrt{\omega}}. \tag{B5}$$

Now completing the square with respect to z_1 and replacing z_1 by u as

$$u=\sqrt{1+a^2}z_1-\chi(x_1,\omega)\quad\text{and}\quad\chi(x_1,\omega)=\frac{a\,(a+(x-x_1)/(2\omega))}{\sqrt{1+a^2}},$$

we ultimately obtain from (B5)

$$\frac{P_T}{4\pi\sqrt{1+a^2}}\int_0^\infty\left\{\int_0^\infty\exp\left[-P_T\,(1+\kappa(x_1,\omega))\,\omega\right]\operatorname{erfc}\left[-\sqrt{P_T\omega}\left(\frac{\sqrt{1+a^2}y}{x-x_1}+\chi(x_1,\omega)\right)\right]\right\}\frac{d\omega}{\omega},\quad\text{(B6)}$$

where $\kappa(x_1,\omega)=\chi^2(x_1,\omega)/a^2$.

Three other contributions to I_ζ^T in (2.3) for different signs of variables x and y can be found by analogy with the aforementioned contribution. All of them coincide with the contribution (B6). Therefore, the final result should be quadrupled.

Considering further the tip region (where $x\to 0$ and $y\to 0$), we get from (B6)

$$I_\zeta^T=\frac{P_T}{\pi\sqrt{1+a^2}}\int_0^\infty\left\{\int_0^\infty\exp\left[-P_T\,(1+\tilde\kappa(x_1,\omega))\,\omega\right]\operatorname{erfc}\left[-\sqrt{P_T\omega}\tilde\chi(x_1,\omega)\right]\mathrm{d}x_1\right\}\frac{\mathrm{d}\omega}{\omega},\quad\text{(B7)}$$

where

$$\tilde\chi(x_1,\omega)=\frac{a\,(a-x_1/(2\omega))}{\sqrt{1+a^2}}\quad\text{and}\quad\tilde\kappa(x_1,\omega)=\frac{\tilde\chi^2(x_1,\omega)}{a^2}.$$

Changing again the variables of integration as

$$\omega'=P_T\omega\quad\text{and}\quad x_1'=P_Tx_1,$$

we finally rewrite expression (B7) in the form of

$$\left.\begin{aligned}I_\zeta^T&=\frac{1}{\pi\sqrt{1+a^2}}\int_0^\infty\left\{\int_0^\infty\exp\left[-(1+\kappa')\omega'\right]\operatorname{erfc}\left[-\sqrt{\omega'}\chi'\right]\mathrm{d}x_1'\right\}\frac{d\omega'}{\omega'}\\ \text{and}\qquad\chi'\left(x_1',\omega'\right)&=\frac{a\left(a-x_1'/(2\omega')\right)}{\sqrt{1+a^2}},\ \kappa'\left(x_1',\omega'\right)=\frac{\chi'^2\left(x_1',\omega'\right)}{a^2},\ a<0.\end{aligned}\right\}\quad\text{(B8)}$$

The concentration integral can be easily calculated in the same manner and reads as

$$I_\zeta^C=\frac{(1-k_0)\,C_{l\infty}I_\zeta^T}{1-(1-k_0)\,I_\zeta^T}.\quad\text{(B9)}$$

Expressions (B8) and (B9) determining a three-dimensional angled dendrite do not depend on the Péclet numbers P_T and P_C. These formulae completely correspond to expression (2.11).

References

1. Chernov AA. 1984 *Modern crystallography III – crystal growth*. Berlin, Germany: Springer.
2. Kurz W, Fisher DJ, Trivedi R. 2019 Progress in modelling solidification microstructures in metals and alloys: dendrites and cells from 1700 to 2000. *Int. Mater. Rev.* **64**, 311–354. (doi:10.1080/09506608.2018.1537090)
3. Langer JS, Hong DC. 1986 Solvability conditions for dendritic growth in the boundary-layer model with capillary anisotropy. *Phys. Rev. A* **34**, 1462–1471. (doi:10.1103/PhysRevA.34.1462)
4. Pelcé P, Bensimon D. 1987 Theory of dendrite dynamics. *Nucl. Phys. B* **2**, 259–270. (doi:10.1016/0920-5632(87)90022-3)
5. Ben Amar M, Pelcé P. 1989 Impurity effect on dendritic growth. *Phys. Rev. A* **39**, 4263–4269. (doi:10.1103/PhysRevA.39.4263)
6. Barbieri A, Langer JS. 1989 Predictions of dendritic growth rates in the linearized solvability theory. *Phys. Rev. A* **39**, 5314–5325. (doi:10.1103/PhysRevA.39.5314)
7. Alexandrov DV, Galenko PK. 2015 Thermo-solutal and kinetic regimes of an anisotropic dendrite growing under forced convective flow. *Phys. Chem. Chem. Phys.* **17**, 19 149–19 161. (doi:10.1039/C5CP03018H)

8. Alexandrov DV, Galenko PK. 2017 Dendritic growth with the six-fold symmetry: theoretical predictions and experimental verification. *J. Phys. Chem. Solids* **108**, 98–103. (doi:10.1016/j.jpcs.2017.04.016)
9. Alexandrov DV, Galenko PK. 2017 Selected mode for rapidly growing needle-like dendrite controlled by heat and mass transport. *Acta Mater.* **137**, 64–70. (doi:10.1016/j.actamat.2017.07.022)
10. Alexandrov DV, Galenko PK. 2019 Selection criterion of stable mode of dendritic growth with n-fold symmetry at arbitrary Péclet numbers with a forced convection. In *IUTAM Symposium on Recent Advances in Moving Boundary Problems in Mechanics, IUTAM Bookseries 34* (eds S Gutschmidt, JN Hewett, M Sellier), pp. 203–215. Springer, Cham. (doi:10.1007/978-3-030-13720-5_17)
11. Ivantsov GP. 1947 Temperature field around spherical, cylinder and needle-like dendrite growing in supercooled melt. *Dokl. Akad. Nauk SSSR* **58**, 567–569.
12. Ivantsov GP. 1952 On a growth of spherical and needle-like crystals of a binary alloy. *Dokl. Akad. Nauk SSSR* **83**, 573–575.
13. Alexandrov DV, Galenko PK. 2014 Dendrite growth under forced convection: analysis methods and experimental tests. *Phys.–Usp.* **57**, 771–786. (doi:10.3367/UFNe.0184.201408b.0833)
14. Horvay G, Cahn JW. 1961 Dendritic and spheroidal growth. *Acta Metall.* **9**, 695–705. (doi:10.1016/0001-6160(61)90008-6)
15. Ananth R, Gill WN. 1989 Dendritic growth of an elliptical paraboloid with forced convection in the melt. *J. Fluid Mech.* **208**, 575–593. (doi:10.1017/S0022112089002946)
16. McFadden GB, Coriell SR, Sekerka RF. 2000 Analytic solution for a non-axisymmetric isothermal dendrite. *J. Cryst. Growth* **208**, 726–745. (doi:10.1016/S0022-0248(99)00478-9)
17. Almgren R, Dai W-S, Hakim V. 1993 Scaling behavior in anisotropic Hele-Shaw flow. *Phys. Rev. Lett.* **71**, 3461–3464. (doi:10.1103/PhysRevLett.71.3461)
18. Plapp M, Karma A. 2000 Multiscale random-walk algorithm for simulating interfacial pattern formation. *Phys. Rev. Lett.* **84**, 1740–1743. (doi:10.1103/PhysRevLett.84.1740)
19. Brener E. 1993 Needle-crystal solution in three-dimensional dendritic growth. *Phys. Rev. Lett.* **71**, 3653–3656. (doi:10.1103/PhysRevLett.71.3653)
20. Brener E. 1999 Pattern formation in three-dimensional dendritic growth. *Physica A* **263**, 338–344. (doi:10.1016/S0378-4371(98)00488-9)
21. Nash GE. 1974 Capillary-limited, steady state dendritic growth, Part I — Theoretical development. *NRL Report 7679, May 1974*.
22. Nash GE, Glicksman ME. 1974 Capillary-limited steady-state dendritic growth — I. Theoretical development. *Acta Metall.* **22**, 1283–1290. (doi:10.1016/0001-6160(74)90141-2)
23. Langer JS, Turski LA. 1977 Studies in the theory of interfacial stability — I. Stationary symmetric model. *Acta Metall.* **25**, 1113–1119. (doi:10.1016/0001-6160(77)90199-7)
24. Langer JS. 1977 Studies in the theory of interfacial stability – II. Moving symmetric model. *Acta Metall.* **25**, 1121–1137. (doi:10.1016/0001-6160(77)90200-0)
25. Saito Y, Goldbeck-Wood G, Müller-Krumbhaar H. 1988 Numerical simulation of dendritic growth. *Phys. Rev. A* **38**, 2148–2157. (doi:10.1103/PhysRevA.38.2148)
26. Hou TY, Lowengrub JS, Shelley MJ. 2001 Boundary integral methods for multicomponent fluids and multiphase materials. *J. Comput. Phys.* **169**, 302–362. (doi:10.1006/jcph.2000.6626)
27. Alexandrov DV, Galenko PK. 2017 Boundary integral approach for propagating interfaces in a binary non-isothermal mixture. *Physica A* **469**, 420–428. (doi:10.1016/j.physa.2016.11.062)
28. Galenko PK, Alexandrov DV, Titova EA. 2018 The boundary integral theory for slow and rapid curved solid/liquid interfaces propagating into binary systems. *Phil. Trans. R. Soc. A* **376**, 20170218. (doi:10.1098/rsta.2017.0218)
29. Kessler DA, Koplik J, Levine H. 1988 Pattern selection in fingered growth phenomena. *Adv. Phys.* **37**, 255–339. (doi:10.1080/00018738800101379)
30. Brener EA, Mel'nikov VI. 1991 Pattern selection in two-dimensional dendritic growth. *Adv. Phys.* **40**, 53–97. (doi:10.1080/00018739100101472)
31. Bisang U, Bilgram JH. 1995 Shape of the tip and the formation of sidebranches of xenon dendrites. *Phys. Rev. Lett.* **75**, 3898–3901. (doi:10.1103/PhysRevLett.75.3898)
32. Lamb (Sir) H. 1945 *Hydrodynamics*. New York, NY: Dover.

33. Kochin NE, Kibel' IA, Roze NV. 1964 *Theoretical Hydromechanics*. New York, NY: Interscience.
34. Ovsienko DE, Alfintsev GA, Maslov VV. 1974 Kinetics and shape of crystal growth from the melt for substances with low L/kT values. *J. Cryst. Growth* **26**, 233–238. (doi:10.1016/0022-0248(74)90251-6)
35. Huang S-C, Glicksman ME. 1981 Overview 12: fundamentals of dendritic solidification — II development of sidebranch structure. *Acta Metall.* **29**, 717–734. (doi:10.1016/0001-6160(81)90116-4)
36. Galenko PK, Herlach DH. 2006 Fractals, morphological spectrum and complexity of interfacial patterns in non-equilibrium solidification. In *Complexus mundi: emergent patterns in nature* (ed. MM Novak), pp. 199–208. Hackensack, NJ: World Scientific.
37. Ovsienko DE, Alfintsev GA. 1975 Growth forms of cyclohexanol crystals at different melt temperatures. In *Growth of crystals*, vol. 9 (eds NN Sheftal', EI Givargizov), pp. 184–188. New York, NY: Consultants Bureau. (doi:10.1007/978-1-4684-1689-3_40)
38. Fedorov OP. 2010 *Crystal growth processes: kinetics, formation, inhomogeneities*. Kiev, Ukraine: Naukova Dumka.
39. Karma A, Rappel W-J. 1999 Phase-field model of dendritic sidebranching with thermal noise. *Phys. Rev. E* **60**, 3614–3625. (doi:10.1103/PhysRevE.60.3614)
40. Danilov D, Nestler B. 2004 Dendritic to globular morphology transition in ternary alloy solidification. *Phys. Rev. Lett.* **93**, 215501. (doi:10.1103/PhysRevLett.93.215501)
41. Nestler B, Danilov D, Galenko P. 2005 Crystal growth of pure substances: phase-field simulations in comparison with analytical and experimental results. *J. Comput. Phys.* **207**, 221–239. (doi:10.1016/j.jcp.2005.01.018)
42. Dougherty A, Gollub JP. 1988 Steady-state dendritic growth of NH_4Br from solution. *Phys. Rev. A* **38**, 3043–3053. (doi:10.1103/PhysRevA.38.3043)
43. Karma A, Rappel W-J. 1997 Phase-field simulation of three-dimensional dendrites: is microscopic solvability theory correct?. *J. Cryst. Growth* **174**, 54–64. (doi:10.1016/S0022-0248(96)01060-3)
44. Karma A, Rappel W-J. 1998 Quantitative phase-field modeling of dendritic growth in two and three dimensions. *Phys. Rev. E* **57**, 4323–4349. (doi:10.1103/PhysRevE.57.4323)
45. Alexandrov DV, Galenko PK, Toropova LV. 2018 Thermo-solutal and kinetic modes of stable dendritic growth with different symmetries of crystalline anisotropy in the presence of convection. *Phil. Trans. R. Soc. A* **376**, 20170215. (doi:10.1098/rsta.2017.0215)
46. Pelcé P. 1988 *Dynamics of curved fronts*. Boston, MA: Academic Press.
47. Li Q, Beckermann C. 1998 Scaling behavior of three-dimensional dendrites. *Phys. Rev. E* **57**, 3176–3188. (doi:10.1103/PhysRevE.57.3176)
48. Melendez AJ, Beckermann C. 2012 Measurements of dendrite tip growth and sidebranching in succinonitrile–acetone alloys. *J. Cryst. Growth* **340**, 175–189. (doi:10.1016/j.jcrysgro.2011.12.010)
49. Brener EA, Temkin DE. 1989 Dendritic growth at deep undercooling and transition to planar front. *Europhys. Lett.* **10**, 171–175. (doi:10.1209/0295-5075/10/2/014)
50. Galenko PK, Krivilyov MD, Buzilov SV. 1997 Bifurcations in a sidebranch surface of a free-growing dendrite. *Phys. Rev. E* **55**, 611–619. (doi:10.1103/PhysRevE.55.611)
51. Alexandrov DV, Titova EA, Galenko PK. 2019 A shape of dendritic tips at high Péclet numbers. *J. Cryst. Growth* **515**, 44–47. (doi:10.1016/j.jcrysgro.2019.03.008)
52. Dougherty A, Lahiri M. 2005 Shape of ammonium chloride dendrite tips at small supersaturation. *J. Cryst. Growth* **274**, 233–240. (doi:10.1016/j.jcrysgro.2004.09.065)
53. Maurer J, Bouissou P, Perrin B, Tabeling P. 1989 Faceted dendrites in the growth of NH_4Br crystals. *Europhys. Lett.* **8**, 67–72. (doi:10.1209/0295-5075/8/1/012)
54. Gradshteyn IS, Ryzhik IM. 2007 *Tables of integrals, series, and products*. New York, NY: Academic Press.